University Library

MINERVA ACCESS

A gateway to Melbourne's research publications

Minerva Access is the Institutional Repository of The University of Melbourne

Author/s:
Davenport, AJ;Cross, RS;Watson, KA;Liao, Y;Shi, W;Prince, HM;Beavis, PA;Trapani, JA;Kershaw, MH;Ritchie, DS;Darcy, PK;Neeson, PJ;Jenkins, MR

Title:
Chimeric antigen receptor T cells form nonclassical and potent immune synapses driving rapid cytotoxicity

Date:
2018-02-27

Citation:
Davenport, A. J., Cross, R. S., Watson, K. A., Liao, Y., Shi, W., Prince, H. M., Beavis, P. A., Trapani, J. A., Kershaw, M. H., Ritchie, D. S., Darcy, P. K., Neeson, P. J. & Jenkins, M. R. (2018). Chimeric antigen receptor T cells form nonclassical and potent immune synapses driving rapid cytotoxicity. Proceedings of the National Academy of Sciences of the United States of America, 115 (9), pp.E2068-E2076. https://doi.org/10.1073/pnas.1716266115.

Persistent Link:
https://hdl.handle.net/11343/253195

License:
CC BY-NC-ND

Chimeric antigen receptor T cells form nonclassical and potent immune synapses driving rapid cytotoxicity

A. J. Davenport[a,b], R. S. Cross[a,c,d], K. A. Watson[c,d], Y. Liao[d,e], W. Shi[e,f], H. M. Prince[a,b], P. A. Beavis[a,b], J. A. Trapani[a,b], M. H. Kershaw[a,b], D. S. Ritchie[g,h], P. K. Darcy[a,b,1,2], P. J. Neeson[a,b,1,2], and M. R. Jenkins[a,b,c,d,i,1,2]

[a]Cancer Immunology Research, Peter MacCallum Cancer Center, Melbourne, VIC 3000, Australia; [b]Sir Peter MacCallum Department of Oncology, The University of Melbourne, Parkville, VIC 3000, Australia; [c]Immunology Division, The Walter and Eliza Hall Institute of Medical Research, Parkville, VIC 3052, Australia; [d]Department of Medical Biology, The University of Melbourne, Parkville, VIC 3052, Australia; [e]Bioinformatics Division, The Walter and Eliza Hall Institute of Medical Research, Parkville, VIC 3052, Australia; [f]Department of Computing and Information Systems, The University of Melbourne, Parkville, VIC 3010, Australia; [g]Australian Cancer Research Foundation Translational Research Laboratory, Melbourne Health, Parkville, VIC 3050, Australia; [h]Department of Medicine, The University of Melbourne, Parkville, VIC 3010, Australia; and [i]Institute for Molecular Science, LaTrobe University, Bundoora, VIC 3086, Australia

Edited by Ronald N. Germain, National Institutes of Health, Bethesda, MD, and approved January 16, 2018 (received for review September 24, 2017)

Chimeric antigen receptor T (CAR-T) cells are effective serial killers with a faster off-rate from dying tumor cells than CAR-T cells binding target cells through their T cell receptor (TCR). Here we explored the functional consequences of CAR-mediated signaling using a dual-specific CAR-T cell, where the same cell was triggered via TCR (tcrCTL) or CAR (carCTL). The carCTL immune synapse lacked distinct LFA-1 adhesion rings and was less reliant on LFA to form stable conjugates with target cells. carCTL receptors associated with the synapse were found to be disrupted and formed a convoluted multifocal pattern of Lck microclusters. Both proximal and distal receptor signaling pathways were induced more rapidly and subsequently decreased more rapidly in carCTL than in tcrCTL. The functional consequence of this rapid signaling in carCTL cells included faster lytic granule recruitment to the immune synapse, correlating with faster detachment of the CTL from the target cell. This study provides a mechanism for how CAR-T cells can debulk large tumor burden quickly and may contribute to further refinement of CAR design for enhancing the quality of signaling and programming of the T cell.

chimeric antigen receptor | cell death | cytotoxicity | cytotoxic T lymphocyte | immune synapse

Chimeric antigen receptor T (CAR-T) cells show great promise in the clinic with objective responses and increased relapse free survival in patients with refractory pediatric B-cell acute lymphoblastic leukemia (B-ALL), adult B-ALL, and non-Hodgkin lymphoma (1–4) and very recently in glioblastoma (5). However, clinical responses to date in other hematological and solid cancers have been sporadic (reviewed in ref. 6). There are many potential causes for these observations, including (*i*) inadequate trafficking of CAR-T cells to the tumor, (*ii*) lack of CAR-T cell persistence, (*iii*) tumor microenvironment-induced immune suppression, and (*iv*) loss of CAR expression in vivo impacting functional response to tumor antigen.

In many patients with refractory disease the CAR-T cell dose used in successful treatments was far smaller than the tumor burden, indicating that CAR-T cells may have proliferated in vivo (7). Our recent data showed that CAR-T cells can mediate rapid and serial killing of tumor cells, indicating that, in addition to CAR-T proliferation, multiple functional pathways may potentially contribute to the dramatic responses observed in some CAR-T cell clinical trials (8). A strong CAR-T cell response in vivo is dependent on stable expression of the CAR, recognition of cognate antigen on tumor cells, and subsequent activation of the effector cell. Activation of a cytotoxic T cell (CTL) is initiated after formation of an immune synapse (IS), a highly organized structure formed at the interface between effector and target cells (9, 10). The TCR-initiated IS comprises a series of concentric rings of clustered molecules (termed supramolecular activating clusters, or SMAC) (10), where each SMAC confers a specific function. The TCR and Lck are clustered in the central SMAC, or cSMAC, while the LFA-1 adhesion molecule and its adaptor talin are located in the peripheral SMAC, or pSMAC (10, 11). Immunofluorescence imaging revealed that actin accumulates to the distal SMAC (dSMAC), to create the well-known bulls-eye synapse structure (12). Thus, organization of the IS is important as each SMAC confers a function. In the cSMAC, the accumulation of activatory signaling enhances and reinforces the initial response (13, 14). In addition, the cSMAC is the delivery site for cytotoxic granules just before delivery of the lethal hit (12). The adhesion ring present in the pSMAC stabilizes the IS via LFA-1 integrin-mediated binding to ICAM-1 on target cells (15).

In contrast to the IS formed via TCR activation, the IS formed by ligation of the CAR in T cells is completely understudied. In addition, the ensuing signaling events leading to CAR-T cell activation are only partially described. A recent study reported phosphorylation of ZAP70 when HEK-CAR19 cells were conjugated with the $CD19^+$ Raji cell line (16). Other studies have demonstrated increased PI3K activity, phospho-AKT levels (17), and T cell survival proteins (18) by third-generation CARs compared with second-generation CARs following antigen stimulation. However, the kinetics and duration of CAR-mediated signaling and the implications for CAR-T cytotoxicity efficiency is not known. To address these issues we used a dual-receptor CAR-T cell model, where the OTI TCR specific for SIINFEKL peptide in association with

Significance

Davenport et al. discovered that the chimeric antigen receptor (CAR) immune synapse structure is different from the T cell receptor (TCR) synapse. The CAR immune synapse formed a disorganized pattern of Lck and more rapidly recruited lytic granules compared with the TCR. The differing immune synapse correlated with faster killing of tumor target cells and detachment from dying tumor cells by CAR-T cells. These findings provide a mechanism whereby CAR-T cells can effectively reduce large tumor burden in patients. This study will form a basis upon which to compare future receptor design to modulate signaling and programming of cytotoxic CAR-T cells to improve treatment of solid cancers.

Author contributions: A.J.D., P.K.D., P.J.N., and M.R.J. designed research; A.J.D., R.S.C., K.A.W., and M.R.J. performed research; P.K.D., P.J.N., and M.R.J. contributed new reagents/analytic tools; A.J.D., Y.L., W.S., P.K.D., P.J.N., and M.R.J. analyzed data; and A.J.D., H.M.P., P.A.B., J.A.T., M.H.K., D.S.R., P.K.D., P.J.N., and M.R.J. wrote the paper.

The authors declare no conflict of interest.

This article is a PNAS Direct Submission.

This open access article is distributed under Creative Commons Attribution-NonCommercial-NoDerivatives License 4.0 (CC BY-NC-ND).

[1]P.K.D., P.J.N., and M.R.J. contributed equally to this work.

[2]To whom correspondence may be addressed. Email: phil.darcy@petermac.org, paul.neeson@petermac.org, or jenkins.m@wehi.edu.au.

This article contains supporting information online at www.pnas.org/lookup/suppl/doi:10.1073/pnas.1716266115/-/DCSupplemental.

Published online February 12, 2018.

H-2K^b and a second-generation anti-HER2 CAR (CD28-CD3ζ) were expressed in the same CD8$^+$ T cell (8). This enabled us to compare, within the same cell, TCR (tcrCTLs) versus CAR-initiated (carCTLs) IS structure, signaling, and the downstream effect on tumor target killing efficiency.

Results and Discussion

The carCTL IS Is Not Conventional. We previously showed that carCTLs detached faster than tcrCTL from dying target cells (8). To explore the mechanisms for this observation we first examined the ability of CAR-T cells to form conjugates with OVA_{257}- or HER2-expressing EL4 tumor targets. In a standard conjugate assay a significantly higher percentage of tcrCTL, compared with carCTL, formed conjugates with tumor cells from 10 to 40 min (Fig. 1*A*). These results are consistent with more rapid carCTL detachment from tumor cells up to 40 min (Fig. 1*A*), supporting our previously published observations of a faster "off-rate" when viewed by live cell microscopy (8). These off-rates are associated with the avidity of CTL-target interactions. In our model, the number of target cell antigen (HER2 or H-2K^b MHCI) molecules were equivalent (8); therefore, the interactions described in this paper compare interactions with a similar number of interacting ligands.

It is well established that TCR signals activate LFA-1, which in turn promotes T cell signaling in the synapse and T cell activation. In vivo, LFA-1 is important for T cell homing and trafficking, with variable levels of LFA-1 having been found on tumor-infiltrating lymphocytes in melanoma tumors (19). Flow cytometry-based conjugate assays are able to detect stable conjugate formation, formed by CTL TCR/CAR interactions as well as LFA-1 binding to its ligand (ICAM-1) on tumor cells.

Using a conjugate assay we determined the level of stable immune synapse formed by tcrCTLs or carCTLs and the role of LFA-1 in forming these stable ISs (Fig. 1 *A* and *C*). The tcrCTLs formed significantly more conjugates than carCTLs from 10 to 40 min, suggesting that tcrCTL conjugates were more stable than those formed by carCTL (Fig. 1*A*). tcrCTL conjugate formation was significantly more dependent on the presence of LFA-1 than carCTL (Fig. 1 *A* and *C*, *i*). This indicates that carCTL are not as dependent on LFA-1 for synapse formation. Furthermore, while the tcrCTL IS had a distinct LFA-1 adhesion ring the carCTL IS was characterized by a disorganized LFA-1 pattern (Fig. 1*B*).

It has previously been shown that three TCR–MHC interacting molecules are sufficient to trigger cytotoxicity by OTI CTLs; however, LFA-1 clustering (as measured by ICAM-1–GFP) required 8 to 10 peptide-loaded MHC (pMHC) complexes for stable ring formation (20). This indicates that formation of a classical stable IS is not always required for cytotoxicity. Furthermore, in our model system carCTLs may bypass the formation of the stable IS structure to induce tumor-cell killing. Single-molecule imaging techniques have shown that a single pMHC ligand is sufficient to trigger TNFα and IL-2 secretion by CD4$^+$ T cells (21). However, it is not known whether CD4$^+$ or CD8$^+$ carCTLs require formation of a stable synapse structure for cytokine production.

Despite equivalent killing by CAR.OTI CTL of either OVA- or HER2-expressing target cells there was no effect on the percentage of target cell killing through the TCR or CAR when LFA-1 was blocked, indicating efficient cytotoxic granule delivery (Fig. 1 *C*, *ii*). Consistent with this data, live-cell imaging demonstrated the capacity of carCTLs to induce cytotoxicity of MC57-HER2 target cells in the presence of LFA-1 blocking antibody (Fig. S1 and Movie S1). Therefore, despite data suggesting that LFA-1 is involved in the polarization of lytic granules in natural killer cells (22), LFA appears to be redundant for both tcrCTL- and carCTL-mediated cytotoxicity by CAR.OTI CTLs (Fig. 1 *C*, *ii*).

A striking observation in this study was that the gross molecular structure of the carCTL IS was found to be different from the conventional tcrCTL synapse (Fig. 1*D*). Lck is a proximal signaling molecule recruited to the TCR for activation. In a conventional tcrCTL IS, Lck clusters to the cSMAC, surrounded by an LFA-1 ring, that is usually important for CTL adhesion. In contrast, the IS structure of the carCTL was characterized by a lack of Lck clustering and displayed Lck patches in a disorganized pattern (Fig. 1*D*). To determine whether this lack of Lck clustering was specific to the CAR or was dependent on antigen specificity we examined Lck at the IS of T cell synapses triggered by a CAR of alternate specificity. A similar second-generation CAR construct, differing only in the single chain specificity for carcinoembryonic antigen (CEA), was used to transduce OTI T cells and Lck examined by immunofluorescence. CEA-specific carCTLs displayed the same lack of organized Lck clustering at the IS (Fig. S2), indicating that carCTLs display an inherent difference from tcrCTLs in the IS structure.

Following quantitation the proportion of carCTLs with accumulation of Lck microclusters and actin rings was found to be significantly reduced, compared with tcrCTLs (Fig. 1*E*). Measurements across the IS of the actin clearance inner diameter revealed that tcrCTLs and carCTLs both formed equivalent synapse sizes at 5 min; however, the carCTL synapse size was significantly smaller than that formed by tcrCTLs at 20 min (Fig. 1*E*). These data indicated that the carCTL IS duration was shorter than the tcrCTL IS. This correlated with the faster carCTL off-rate (8), a smaller IS characterized by actin-rich accumulation and protrusions, as well as microclusters of proximal Lck signaling (Fig. 1 *D* and *E* and Fig. S2). Our data are supported by previous studies including a report by James and Vale (16) who demonstrated clustering of CD19-specific CARs in a reconstituted HEK cell line recognizing CD19+ -Raji B target cells with a highly convoluted membrane surface at the IS. This is also consistent with another paper reporting CD19-CAR clustering and actin accumulation at the IS (23).

The TCR IS initiates phosphorylation of proximal (Lck and ZAP-70) and distal (ERK) signaling proteins (13) and is critical for CTL assembly of the cytotoxic machinery (12) and killing of target cells. However, these characteristics of the CAR IS signaling network and its effect on cytotoxicity are unknown.

carCTLs Induce Rapid Proximal Signaling of Shorter Duration than tcrCTLs. Given the differences observed in Lck clustering at the IS we next examined Lck phosphorylation in carCTLs and tcrCTLs in response to cognate antigen. Western blot analysis revealed a rapid twofold increase in phospho-Lck (pLck) protein expression by 2 min in carCTL following antigen stimulation that decreased to the level induced in tcrCTLs by 10 min (Fig. 2*A*). The distal phospho-ERK (pERK) protein expression was also found to be increased in carCTLs at 2 min and 10 min following antigen stimulation and remained stable for 30 min (Fig. 2*B*). Calcium increase in the cytoplasm of CTLs is an early indicator of proximal TCR signaling and antigen recognition. We consistently found that carCTLs exhibited fewer Ca^{2+} fluxes before the propidium iodide (PI) blush (Fig. 2*C*, *Left*), consistent with our previous findings (24).

To determine whether increased pLCK and pERK led to any change in the intensity of the Ca^{2+} flux we next compared this in carCTLs and tcrCTLs following antigen-specific activation (Fig. 2*C*). Interestingly, there was no difference observed in the Ca^{2+} flux intensity between carCTLs and tcrCTLs following antigen-specific activation (Fig. 2*C*), indicating that a threshold level of activation had occurred and that this is not enhanced in carCTL. Taken together, these data indicate that signaling is stronger, more rapid, and of shorter duration in carCTL than in tcrCTL. Given the fact that a sustained tcrCTL signal is required for cytokine production, we next examined whether there was any

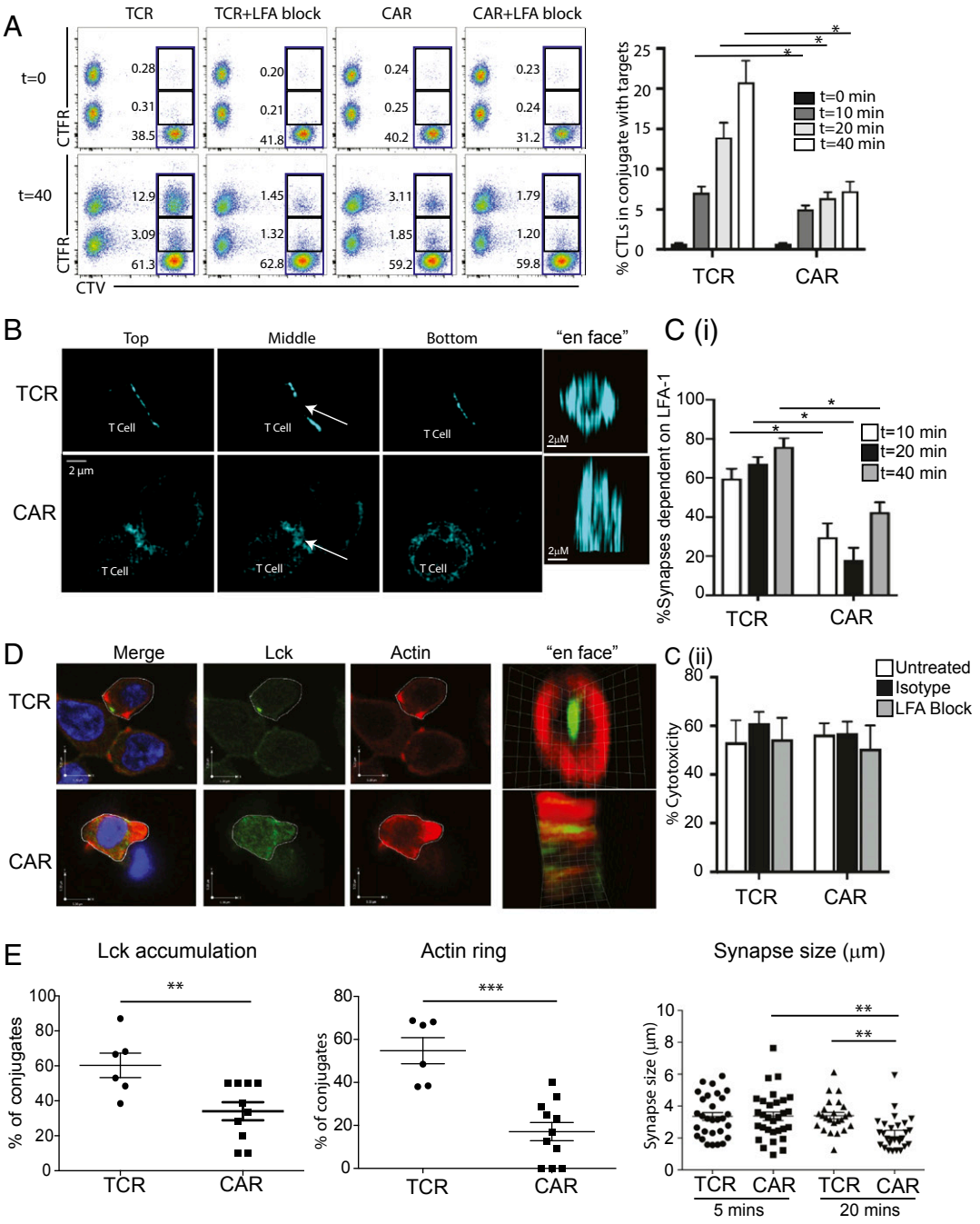

Fig. 1. carCTL synapses are smaller and lack a defined Lck patch. (*A*) Flow cytometry plots (*A*, *Left*) of CTV-labeled effector CAR.OTI CTLs cocultured with EL4 target cells and EL4HER2 (CAR) or EL4OVA$_{257}$ (TCR) each labeled with CTFR^{hi} or parental EL4 (CTFR^{lo}). This conjugate assay was also performed in the absence or presence of LFA-1 blocking antibody. Cells forming conjugates were analyzed over 40 min. The graph (*A*, *Right*) shows percentage of CD8$^+$ T cells forming conjugates with targets (mean ± SD) where each condition was performed in triplicate. The figure shows pooled data from four independent experiments. *$P < 0.05$ as determined by a Student's *t* test. (*B*) Confocal microscopy of CAR.OTI cells in conjugation with MC57 target cells via TCR or CAR, labeled with anti-LFA-1. Montage of confocal planes are shown across the top, middle, and bottom of the T cell. (*C*, *i*) Conjugate assay showing the percentage of synapses dependent on LFA-1 binding relative to normal kinetics. CTV-labeled CAR.OTI CTLs were incubated with CTFR-labeled EL4-OVA$_{257}$ (TCR) or EL4-Her2 (CAR) before being analyzed by flow cytometry. CD8$^+$ T cells (CTV) still in synapse with target (CTVhi/CTFRhi) are compared with proportion of cells in synapse in the presence of LFA-1 blocking antibody and shown is the proportion of total synapses which are lost when LFA-1 is blocked. Data are an average of three independent experiments, pooled, showing mean ± SEM and statistical differences between TCR and CAR at each time point determined by Student's *t* test, *$P < 0.05$. (*C*, *ii*) Chromium release killing assay. Activated CAR.OTI cells were incubated with ^{51}Cr-labeled MC57-OVA (TCR) or MC57-HER2 (CAR) cells, in the presence of media alone (Untreated, white), isotype control antibody (Isotype, black), or anti-CD11a blocking antibody (LFA Block, Gray) for 5 h at 1:10 E:T ratio, before measuring ^{51}Cr-release. Data represent the percentage of tumor cell lysis (mean ± SD) from two independent experiments. (*D*) Confocal microscopy of CAR.OTI cells in conjugation with MC57 target cells via TCR or CAR, labeled with anti-Lck (green), anti-actin (red), and Hoechst (blue). (*E*) ISs as shown in *D* were blindly quantitated using an unbiased approach for the percentage of conjugates displaying a complete discrete Lck patch at the IS, a cleared actin ring, and the size of the actin ring in conjugates after 5 or 20 min of conjugation. Each data point represents a field of view ($n > 6$) with at least 8–10 conjugates from each (therefore >48 cells), from more than three biological replicate experiments. Student's *t* test showed statistical differences *$P < 0.05$, **$P < 0.01$, ***$P < 0.001$ as indicated.

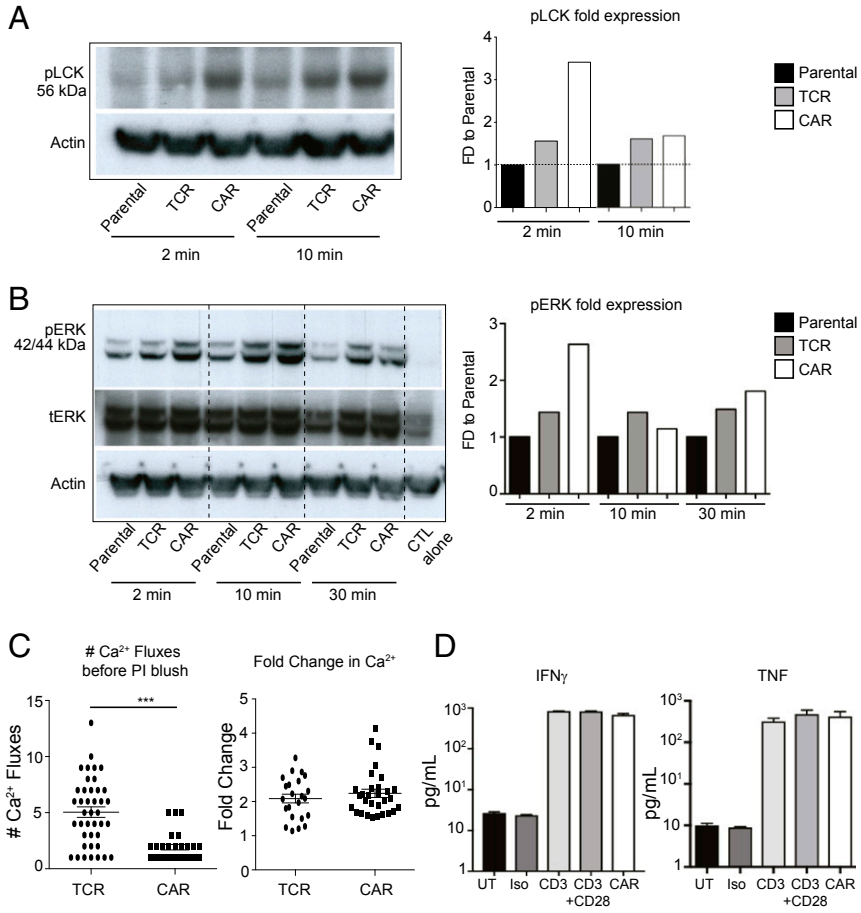

Fig. 2. CAR ligation initiates faster proximal and distal T cell signaling than TCR ligation. CAR.OTI CTLs cocultured with parental, OVA_{257}-, or HER2-expressing MC57 targets and Western blotting performed for (*A*) pLck; (*B*) pErk, total Erk; and actin. Quantitation utilized Fiji imaging software and was normalized to actin loading. Data represented in graphs as mean fold change from parental expression. Western blots are representative of two (*A*) and three (*B*) experiments. FD, fold difference. (*C*) Effector CAR.OTI CTLs were labeled with Fluo4-AM and added to adherent MC57 cells expressing either the TCR antigen (OVA_{257}) or the CAR antigen (HER2) and imaged using live-cell microscopy. Individual conjugates were quantitated for the time taken after T cell calcium flux until PI entering the target cell cytosol and the fold change in Ca^{2+} intensity, as measured by Fluo-4-AM MFI. Each point represents one conjugate and data pooled from three independent experiments. Student's *t* test, $^{***}P < 0.001$. (*D*) CAR.OTI CTLs were added to plates precoated with either PBS (UT), isotype control (Iso), anti-CD3, anti-CD3 + anti-CD28, or anti-myc-tag (CAR). Supernatant was collected after 5 h and analyzed for IFN-γ and TNF levels. Cytokine expression levels (mean ± SEM) in picograms per milliliter of three independent pooled experiments are shown. Statistical significance was determined using Student's *t* test between groups, $^{*}P < 0.05$.

difference in IFN-γ and TNFα secretion from carCTL and tcrCTL following activation. The second-generation CAR used in this study contains the CD28 and CD3ζ endodomains, and therefore we activated CAR.OTI CTLs via either the TCR alone, TCR and CD28, or the CAR (via the c-myc tag domain). However, regardless of stimulation conditions, similar levels of both IFN-γ and TNF were produced (Fig. 2*D*).

To further explore differences between carCTL and tcrCTL signaling we employed a large-scale reverse-phase 308 protein array to identify any signaling pathways that were differentially activated. We found no significant difference in signaling protein expression at 2 min; however, at 30 min, 43 of 308 proteins in tcrCTL versus carCTL were significantly changed (Fig. 3*A*). Out of the 43 differentially expressed proteins we identified signature proteins that are involved in TCR signaling pathways, protein trafficking, and cell survival and proliferation (Fig. 3*B*). Interestingly, the proximal signaling protein PKCδ, which has previously been shown to localize to the secretory lysosomes in CD8 T cell killing (25), was down-regulated in carCTLs compared with tcrCTLs by 30 min, supported by a similar reduction in downstream phosphorylation of JNK and ERK pathways. This suggested that carCTL signaling is more rapid and of shorter duration compared with tcrCTLs. Despite this shorter signaling duration carCTLs maintained a higher expression of both Bcl-2 and PEA-15 over 30 min (Fig. 3*B*). The cellular functions of PEA-15 are yet to be fully elucidated, but it has been previously shown that PEA-15 can negatively regulate ERK1/2, the Fas-associated death domain, and phospholipase D1 proteins, indicating that it may have antiapoptotic, antiproliferative, and antiinflammatory properties (26). Overexpression of BCL2 has also been shown to enhance the therapeutic efficacy of tumor-specific T cells (27). How CAR signaling affects levels of *Bcl-2* or the long-term survival of T cells has yet to be determined. cMET is a receptor tyrosine kinase which activates a large range of cellular pathways including PLCγ1 and PI3K and was down-regulated in carCTLs compared with tcrCTLs. We validated these differences in distal ERK signaling using Western blot analysis, which showed a rapid decrease in phospho-ERK levels by 30 min in carCTLs (Fig. 3*C*). Taken together, these data confirm our observations in the tumor coculture system that CAR-initiated signaling is more rapid and resolves faster than signaling through the TCR. This may have functional sequelae in carCTL, including altered kinetics of cytotoxic granule movement compared with that in tcrCTL.

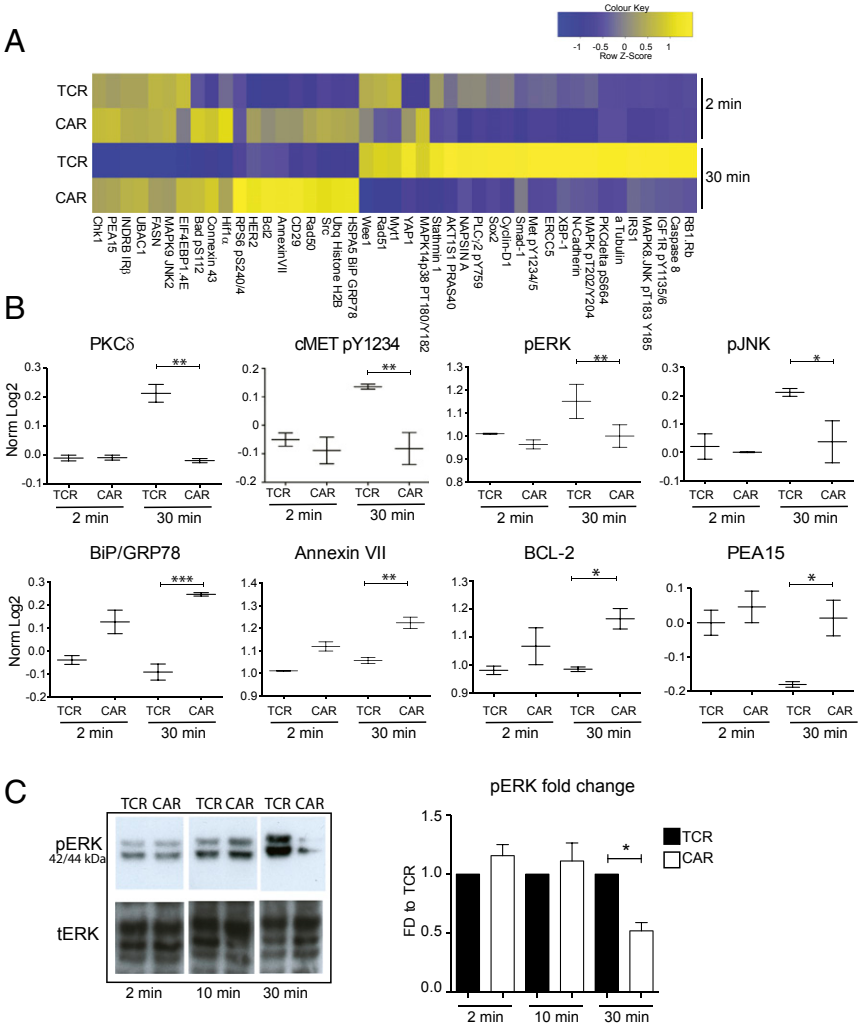

Fig. 3. Proximal signaling dissipates more quickly in carCTL than in tcrCTL. (*A*) RPPA analysis of CAR.OTI CTL signaling at 2 min and 30 min after plate-bound TCR or CAR stimulation. The 43 proteins included in the heat map all have statistically significant changes at 30 min. Blue and yellow represent down- and up-regulation, respectively. Relative protein levels (Z-scores) are shown in the heat map, color-coded according to the legend. Columns are scaled to have a mean of 0 and an SD of 1. (*B*) Quantitated graphical analysis from *A* of select proteins involved in T cell signaling, cell survival, or membrane trafficking. (*C*) Western blot validation of pErk expression from *B*. Western blot analysis probing for pErk at 2 min, 10 min, and 30 min of CAR.OTI stimulation with solid-phase anti-CD3 (TCR) or anti-tag (CAR). The pERK level was normalized to total amount of protein and represented as fold difference to TCR expression at each time point. Student's *t* test, $*P < 0.05$.

Cytotoxic Granules Were Recruited Faster When Signaling via CAR. Upon TCR ligation, CTLs rapidly polarize their cytotoxic machinery toward the site of proximal signaling at the IS. The secretory granules associate with microtubules and are reoriented from the rear of a migrating cell toward the microtubule-organizing center (MTOC), where they dock at the IS and are secreted into the synaptic cleft (12). Cytotoxic granule cargo includes perforin and granzymes, which are essential for inducing target-cell apoptosis, reviewed in ref. 28. We used live-cell microscopy to visualize the kinetics of cytotoxic granule recruitment to the IS in carCTLs and tcrCTLs, prelabeled with a calcium indicator as a marker of antigen recognition (Fig. 4*A*). We showed that after Ca^{2+} flux carCTL recruited cytotoxic granules to the IS faster and with an increased velocity (Fig. 4*B* and Movie S2). In addition, following delivery of the granules to the IS, the carCTL detached from dying tumor cells faster, consistent with our previous published observations (8). Importantly, when examined at the single-cell level, once granules had been delivered by tcrCTLs or carCTLs the target cell took the same amount of time to display signs of apoptosis (e.g., membrane "blebbing"). Therefore, target cells did not die more rapidly when "hit" via a carCTL versus tcrCTL (Fig. 4*B*).

We confirmed the essential role of the MTOC in granule delivery with a loss of cytotoxicity in the presence of the MTOC inhibitor (PKCzIn) (Fig. S3*A*). As expected, despite equivalent cytotoxicity (8) mediated by carCTL and tcrCTLs, by 30 min the MTOC had moved away from the IS in carCTL (Fig. S3 *B* and *C*). This supported our data that cytotoxic granule delivery was faster and the IS resolves more quickly for carCTL. This hypothesis is also consistent with the proposal that TCR triggering initiates low-level Lck phosphorylation which is strengthened after centrosome translocation to the synapse, as observed in live-cell microscopy analysis (29). In contrast, in this study we showed that stronger pLck signaling through the CAR initiates faster lysosome recruitment, and by inference faster migration of the centrosome to the IS. These data support previous studies which showed that higher avidity of TCR for antigen results in enhanced polarization of cytotoxic machinery (30). In another study, low-avidity tumor antigen-specific CTLs can strip pMHC complexes without inducing cytolysis, therefore resulting in

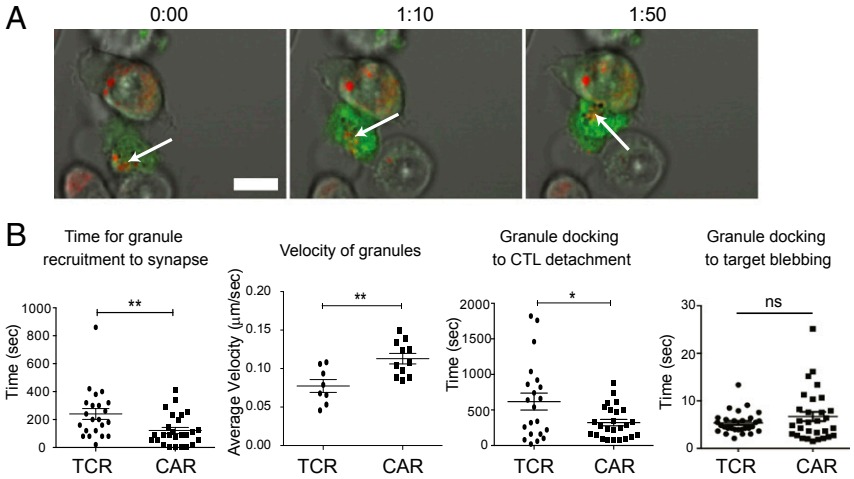

Fig. 4. CAR ligation results in faster granule recruitment to the IS. Effector CAR.OTI CTLs were labeled with Fluo4-AM and lysotracker red, added to adherent MC57 cells expressing either the TCR antigen (OVA_{257}) or the CAR antigen (HER2), and imaged using live-cell microscopy. (*A*) Representative montage of a carCTL conjugate polarizing granules toward the IS. White arrow highlights granules. Time in minutes:seconds. (Scale bar: 10 μm.) (*B*) Individual conjugates were quantitated for the time taken after calcium flux for granule mass to be recruited to the IS, the velocity of the granule mass, and the time from granule recruitment to CTL detachment. Each point represents one conjugate and data pooled from three independent experiments. Student's *t* test ,$^{**}P < 0.001$, $^{*}P < 0.01$. See Movie S2.

insufficient antigen present for high-avidity T cells to initiate cytotoxicity (31). Whether or not CARs with different affinities and avidities will affect the kinetics of cytotoxicity is yet to be determined. However, this may be an essential feature to consider for designing better CAR-T responses.

Concluding Remarks

Our study compares CAR and TCR ligation events in the same T cell. Taken together, our dual-receptor CAR-T cell model revealed a number of distinct features of CAR-T cell IS structure, signaling, and cytotoxic functional responses which were different depending upon which receptor encountered antigen. This is summarized in Fig. 5. carCTL detection of cognate antigen initiated an alternate IS characterized by a disorganized multifocal pattern of Lck arrangement, confirming previous reports of a convoluted synaptic structure (16), a small actin ring, and diffuse LFA-1 distribution (Fig. 5*B*). This was in stark contrast to the IS structure observed in tcrCTL that comprised a classic bull's-eye structure with a peripheral LFA-1 adhesion ring (Fig. 5*A*). Work over the past decade has highlighted the importance of endosomal trafficking of Lck as a critical mediator of T cell signaling (32–34). Alcover and coworkers (35) have suggested that Rab11 interacting with family members such as FIP3 (Rab11 family interacting protein-3) controls Lck trafficking to the IS through its interaction with dynein and microtubules. Therefore, when assessing the disrupted Lck labeling at the IS in our studies we cannot rule out Lck localization at an intracellular pool less than 1 μm from the plasma membrane.

In our previous publication we showed that carCTLs displayed a faster time to detach from dying target cells compared with tcrCTLs. Here we show that the carCTL IS-initiated signaling was more rapid but of shorter duration than that observed for tcrCTL (Fig. 5*C*). This rapid carCTL signaling induced an accelerated delivery of cytotoxic granules to the IS, leading to faster killing of tumor targets. The carCTL displayed an exquisite killing function, induced by a signal of shorter duration (Fig. 5*C*), and a lack of LFA-1 clustering. Together this enabled the carCTL to detach from the dying tumor cell faster and move on to the next tumor target (serial killing). In contrast, the tcrCTL classic IS structure drove a slower, more protracted signaling resulting in slower but more extended killing.

CAR-T cell functional responses are heavily influenced by CAR design, including the scFv affinity for antigen, spacer length, and signaling endodomains (reviewed in ref. 36). Future studies exploring the effect of lower-affinity HER2 scFv in the second-generation CAR, coupled with differing signaling endodomains (e.g., CD137), may reveal a CAR-T cell with slower, more protracted signaling and cytotoxic responses, similar to that generated in tcrCTL. The endodomain design of CARs will ultimately influence the programming of the T cell. In recent studies, swapping CD28 with the CD137 costimulatory domain resulted in increased persistence of CAR-T cells (37). Whether or not the initial synapse structure contributes to this remains to be determined. Future studies focusing on the CAR IS in live imaged carCTL interactions or high-resolution structured illumination microscopy would be helpful to elucidate the exact nature of the CAR IS as well as the recruitment and retention of important synaptic molecules. Additionally, based on our findings, the dual-antigen receptor concept in human CAR-T cells could be used to "tune" the CAR-T cytotoxic response to a desired response depending on the disease status resulting in (*i*) a more rapid serial killer (via the CAR) where the disease burden is initially high or (*ii*) a slower but more protracted cytotoxic response (via the TCR), particularly in the case of tumor relapse. In addition, our prior data (8) showed that carCTL responses initiated loss of CAR expression after 20 h and loss of cytotoxic response to tumor. Similar data were also observed with TCR-engineered T cells; however, reexpression of the engineered TCR was observed following stimulation of the endogenous TCR (38). Thus, stimulating carCTL cells via the TCR (e.g., via a vaccine) may induce reexpression of the CAR and recovery of tumor cytotoxic function. Recent reviews have highlighted technologies that could help to quantify the carCTL IS, similar to that of the tcrCTL (23, 39). These technologies include high-speed, live-cell microscopy techniques recently used in TCR cell biology published by Griffiths and coworkers (29).

In conclusion, this study defined the combination of unique factors that drive CAR-T cells to be efficient killers. In doing so, we provide potential mechanisms which contribute to a CAR-T cell dose eradicating large tumor burden or controlling minimal residual disease.

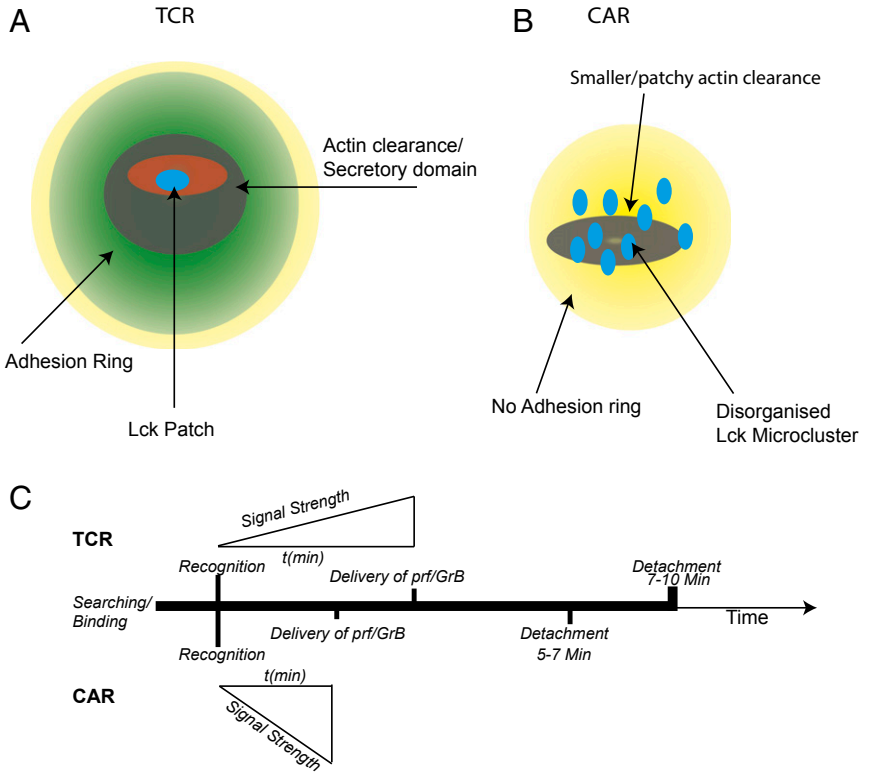

Fig. 5. Schematic model of the CAR and TCR IS and temporal killing event differences. Schematic of the IS in CTLs when activated via the CAR or TCR. (*A*) TCR-mediated conjugates display a classical bull's-eye structure with well-characterized SMAC domains; however, signaling via CAR (*B*) results in disorganized Lck patterns and lack of a pSMAC domain, as labeled by LFA-1 with a smaller actin clearance. (*C*) Timeline depicting temporal differences in killing events by CAR. OTI CTLs when activated by the TCR or CAR.

Materials and Methods

Cell Culture. MC57 (mouse fibrosarcoma cell line), EL4 (mouse T cell thymoma cell line), and their retrovirally transduced derivatives (OVA and Her2) (8) were cultured in complete media: RPMI-1640 comprising 10% FCS, 1 mM sodium pyruvate, 2 mM L-glutamine, 0.1 mM nonessential amino acids, 100 U/mL penicillin/streptomycin (Invitrogen, Life Technologies), and 5 μM 2ME (called cRPMI). All T cell cultures were maintained in cRPMI with the addition of 100 U/mL of recombinant human IL-2 (T cell media).

Antibodies and Reagents. Antibodies for confocal immunofluorescence included the rat anti-mouse LFA-1 (clone C71/10; Biobyt), anti-mouse Lck (clone 3A5; Abcam), rabbit anti-mouse actin (clone 13E5; Cell Signaling), and rabbit anti-mouse γ-tubulin (clone T5192; Sigma). We used Hoechst 33342 from Sigma-Aldrich to counterstain the nucleus. Secondary antibodies included polyclonal goat anti-mouse-488 (A11001), goat anti-rabbit-546 (A11035), and goat anti-rat-647 (Invitrogen). Antibody for the LFA-1 blocking assay was purified rat anti-mouse CD11a (LFA-1α subunit) (clone M17/4; Biolegend) and the corresponding rat IgG2a isotype control (clone GL117; WEHI-Bundoora Antibody Production Facility).

Antibodies for Western blotting included the rabbit anti-pLck (pTyr394) (GTX38561; GeneTex Inc.), rabbit anti-Lck (clone GTX24896; GeneTex Inc.), rabbit anti-PhosphoERK p44/42 (clone D13.14.4E; Cell Signaling Technology), rabbit anti-ERK1/2 p44/42 (clone 137F5; Cell Signaling), and mouse anti-actin (clone 13E5; Cell Signaling). Secondary HRP-conjugated antibodies included anti-rabbit Ig (E0432) and anti-mouse Ig (F0232) (Dako). $OVA_{257–254}$ (SIINFEKL) peptide was obtained from GenScript. CellTrace Violet (CTV), and CellTrace Far Red (CTFR) were obtained from Invitrogen. Reagents used for live-cell imaging studies included Fluo-4–AM (1 μM) and Pluronic F-127 (0.02% wt/vol) (Thermo Fischer) and lysotracker red (DND99 RED, used at 1:1,000; Invitrogen). Protein kinase Cζ pseudosubstrate inhibitor (P1614) (used at 10 μM) was obtained from Sigma-Aldrich.

Mouse Model and Generation of CAR.OTI CTLs. The dual-receptor T cells used in this study have been described previously (8). In brief, the recently described "CAR" mouse model, in which a second-generation CAR (anti-HER2-CD28-CD3ζ) is expressed in all immune system cells under the control of the *vav* promoter (40), was crossed with the OTI mouse to create the CAR.OTI mouse. F1-generation CAR.OTI mouse splenocytes were activated via their TCR as previously reported (41). Briefly, naïve splenocytes were cultured in cRPMI media with 10 nM SIINFEKL peptide and 100 U/mL IL-2 for 3 d. Viable cells were recovered by density gradient centrifugation and cultured for a further 4 d, before being utilized in experiments as activated effector $CD8^+$ T cells (termed CAR.OTI CTL).

Generation of CEA-Specific CAR OTI T Cells. To generate CEA-specific second-generation (anti-CEA-CD28-CD3ζ) dual-specific CAR T cells, OTI mouse splenocytes were activated via their TCR, as described above for 24 h, before being transduced using retrovirus harvested from the GP.E86 viral packaging cell line as previously published (42). Briefly, following activation with 10 nM SIINFEKL peptide, T cells were transduced using spinfection for 1 h at 1,000 × *g*, 22 °C with Retronectin (32 μg/mL). Following transduction, CAR T cells were cultured in cRPMI media with 100 U/mL IL-2 for 5 d before being utilized in experiments as activated effector $CD8^+$ T cells.

Conjugate Assay with LFA-1 Blocking. Preactivated effector CAR.OTI CTLs were labeled with 0.5 μM CTV. Target parental EL4 cells were labeled with 12.5 nM CTFR and EL4-OVA and EL4-Her2 were labeled with 100 nM CTFR. The CTLs were incubated in the presence or absence of 20 μg/mL LFA-1 blocking antibody at 37 °C for 30 min. The targets were added in an equal volume without washing, giving a final ratio of 1:1:1 EL4:EL4-OVA:CAR.OTI or 1:1:1 EL4:EL4-Her2:CAR.OTI. Cell mixtures were incubated for 10, 20, or 40 min at 37 °C, fixed with paraformaldehyde (2% final concentration), washed and analyzed by flow cytometry.

Cytokine Bead Array. Activated CAR.OTI T cells (10^5) were cultured in 96-well flat-bottom plates in T cell media, precoated overnight with PBS, 1 μg mouse IgG2a Isotype control (Cell Signaling) (clone7H8/50), 1 μg/mL anti-CD3 (145-2C11) (BD Biosciences), or 1 μg/mL anti-myc-Tag antibody (9B11; Cell Signaling Technology) for 5 h. Cytokine production was measured from 10 μL of culture supernatant of CTLs using CBA flex sets

(BD Biosciences) for mouse IFN-γ and TNF, according to the manufacturer's instructions. Samples were analyzed on a FACS VERSE using FCAP Array software version 3.0 (Softflow) and the concentration of cytokine was determined to a standard curve and plotted as picograms per milliliter of cytokine.

Confocal Immunofluorescence. Effector CTLs and target cells were resuspended 1:1 in serum-free RPMI at 4×10^6 cells per mL, centrifuged at 200 rpm, and incubated for 5 min 37 °C. Cells were then added to glass multiwell slides (Hendley Slides) and allowed to adhere to glass for 15 min before fixation on ice for 5 min with −20 °C 100% methanol. Slides were then blocked in PBS 2% BSA for 1 h at room temperature and incubated with primary antibodies for 1 h at room temperature and with secondary antibodies for 1 h at room temperature. Nuclei were stained with Hoechst (1:10,000; Sigma-Aldrich) in PBS for 5 min before mounting with 1.5 coverglass and mowiol-mounting medium (Sigma-Aldrich). Slides were examined using a Nikon C2 confocal microscope or Elyra Zeiss Microscope with SIM (63× objective under oil) and lasers exciting at 405 nm (41.5 mW), 488 nm (21.2 mW), and 561 nm (20.2 mW). Image analysis was conducted using MetaMorph Imaging Series 7 software (Universal Imaging), Imaris 7 (Bitplane), or Volocity (PerkinElmer). Images are presented as either single planes or projections, as stated in legends. We used an unbiased blinded approach for the analysis of scoring protein labeling at the IS. For blind scoring of Lck labeling at the IS a 2-μm slice across the IS was isolated for confocal examination, excluding intracellular pools of Lck from the analysis.

T Cell-Signaling Protein Detection. CAR.OTI cells were activated via either (*i*) solid phase antibodies or (*ii*) antigen-expressing tumor target cells. (*i*) CAR.OTI CTLs were cultured at 4×10^6/mL with plate bound antibodies at 1 μg/mL; Armenian hamster anti-CD3e (clone 145-2C11; BD Bioscience), hamster anti-CD28 (clone 37-51; BD Bioscience), or mouse anti-c-myc Tag (clone 9B11; Cell Signaling). (*ii*) CAR.OTI CTLs and MC57 or MC57HER2 tumor target cells were incubated in serum-free media (±1 μM SIINFEKL peptide) for 1 h before coculturing 1:1 and incubating at 37 °C for various time points, before snap freezing (LN_2) in the presence of RIPA buffer (25 mmol/L Hepes, 0.25 mol/L NaCl, 2.5 mmol/L EDTA, and 0.1% Triton X-100), protease inhibitor mixture, and PhosphoStop (Roche Diagnostics). SDS PAGE followed by Western blot was then performed on the cell lysates using a 4–12% Bis-Tris gel (Invitrogen). PVDF membranes were probed with antibodies for 16 h at 4 °C, washed in PBS-T, and probed for 1 h at room temperature with HRP-conjugated secondary antibodies (anti-rabbit Ig or anti-mouse Ig; Dako), washed in PBS-T (3 × 5 min at room temperature) before digital imaging.

Reverse-Phase Protein Array and Bioinformatics Analyses. CAR.OTI CTLs (1×10^7/mL) were transferred to 48-well plates (5×10^6 per well) precoated for 16 h (4 °C) with purified activating antibodies in PBS. Cells from two individual mice were incubated at 37 °C in 5% CO_2 for 2 min, 10 min, or 30 min before being snap-frozen (LN_2) and delivered to the MD Anderson reverse-phase protein array (RPPA) core facility on dry ice. Cell pellets were then lysed in RIPA buffer and serially diluted twofold for five dilutions and arrayed using a nitrocellulose collated slide. Protein lysate samples were probed with antibodies using tyramide-based signal amplification and visualized using DAB-colorimetric reaction. All sample slides were then scanned with a high-resolution scanner and spots from samples were identified and density quantified with Array-Pro Analyzer. Relative protein levels were determined for each dilution curve from a standard curve included on each slide. The standard curve was created in R by the RPPA core at MD Anderson. RPPA staining was performed with 308 different protein antibodies and internally quality-controlled, with a quality control score above 0.8 indicating good antibody labeling. Normlinear data from RPPA analysis was then used to plot graphs in GraphPad Prism. $NormLog_2$ data were converted to their original scale and then quantile-normalized. These normalized values were log2-transformed and fed into the Bioconductor R package limma for linear modeling (43). Protein level changes were assessed using the empirical Bayes moderated-*t* statistic (44). Empirical Bayes moderated-t *P* values were adjusted to control the false discovery rate (FDR). Proteins with significant level changes were called if they achieved a FDR of 0.25 or less. Data shown are a box-and-whiskers plot of $n = 2$ from minimum to maximum.

Time-Lapse Live Microscopy. Interactions between CTLs and tumor cells were assessed by time-lapse live microscopy, using well-established protocols published previously (24, 41, 45). Briefly, adherent MC57- or HER2-expressing MC57 (MC57-HER2) target cells were prepared for live-cell imaging by seeding 3×10^4 cells in each well of an eight-well chamber slide (ibidi) and incubating overnight at 37 °C/10% CO_2. MC57 target cells were then incubated for 1 h with 1 μM SIINFEKL, OVA_{257} peptide. CAR.OTI CTLs (3×10^4 per well) were labeled with Fluo-4-AM and Pluronic F-127 carrier for 20 min at 37 °C/10% CO_2). Lysotracker red was added to each chamber well to monitor granule movement kinetics. To monitor perforation of the target cell membrane 100 μM propidium iodide was added (24). Chamber slides were mounted on a heated stage within a temperature-controlled chamber maintained at 37 °C and constant CO_2 concentrations (5% "The Brick"; ibidi). Optical sections were acquired through sequential scans of Fluo-4 (excitation 488 nm), Lysotracker Red (excitation 561 nm), or Brightfield/DIC on a Leica SP5 confocal microscope (Leica Microsystems) using a 403 (NA 0.85) air objective and Leica LAS AF software. Images were acquired every 20 s. Image analysis was performed using Leica LAS AF Lite software and MetaMorph Imaging Series 7 software (Universal Imaging), Imaris 7 (Bitplane), or Velocity (Perkin-Elmer).

Chromium Release Assay. CAR.OTI CTLs were cocultured with HER2-expressing EL4 cells (5:1 E:T ratio) in a 4-h ^{51}Cr release killing assay (as described previously in ref. 8) in the presence or absence of protein kinase Cζ pseudosubstrate inhibitor (46, 47).

ACKNOWLEDGMENTS. We thank Sarah Ellis, Jill Danne, Chad Johnson, and Kylie Luong for assistance with microscopy; Ralph Rossi, Viki Milovac, and Sophie Curcio for assistance with flow cytometry; the animal facility technicians (Peter MacCallum Cancer Centre) for help with animal care; Melissa Henderson (Peter MacCallum Cancer Centre) for technical support; and Han Xian Aw Yeang for proofreading the manuscript. M.R.J. is supported by a National Health and Medical Research Council of Australia (NHMRC) career development fellowship and an NHMRC New Investigator Project Grant. A.J.D. is supported by a Fight Cancer Foundation PhD Scholarship. J.A.T. and P.J.N. are supported by an NHMRC Program Grant. P.K.D. is supported by an NHMRC Senior Research Fellowship. W.S. is supported by a Walter and Eliza Hall Institute Centenary Fellowship funded by Commonwealth Serum Laboratories.

1. Park JH, Geyer MB, Brentjens RJ (2016) CD19-targeted CAR T-cell therapeutics for hematologic malignancies: Interpreting clinical outcomes to date. *Blood* 127: 3312–3320.
2. Porter DL, et al. (2015) Chimeric antigen receptor T cells persist and induce sustained remissions in relapsed refractory chronic lymphocytic leukemia. *Sci Transl Med* 7: 303ra139.
3. Turtle CJ, et al. (2016) CD19 CAR-T cells of defined CD4+:CD8+ composition in adult B cell ALL patients. *J Clin Invest* 126:2123–2138.
4. Lee DW, et al. (2015) T cells expressing CD19 chimeric antigen receptors for acute lymphoblastic leukaemia in children and young adults: A phase 1 dose-escalation trial. *Lancet* 385:517–528.
5. Brown CE, et al. (2016) Regression of glioblastoma after chimeric antigen receptor T-cell therapy. *N Engl J Med* 375:2561–2569.
6. Yong CSM, et al. (2017) CAR T-cell therapy of solid tumors. *Immunol Cell Biol* 95: 356–363.
7. Kalos M, et al. (2011) T cells with chimeric antigen receptors have potent antitumor effects and can establish memory in patients with advanced leukemia. *Sci Transl Med* 3:95ra73.
8. Davenport AJ, et al. (2015) CAR-T cells inflict sequential killing of multiple tumor target cells. *Cancer Immunol Res* 3:483–494.
9. Kupfer A, Dennert G (1984) Reorientation of the microtubule-organizing center and the Golgi apparatus in cloned cytotoxic lymphocytes triggered by binding to lysable target cells. *J Immunol* 133:2762–2766.
10. Monks CR, Freiberg BA, Kupfer H, Sciaky N, Kupfer A (1998) Three-dimensional segregation of supramolecular activation clusters in T cells. *Nature* 395:82–86.
11. Bromley SK, et al. (2001) The immunological synapse. *Annu Rev Immunol* 19:375–396.
12. Stinchcombe JC, Majorovits E, Bossi G, Fuller S, Griffiths GM (2006) Centrosome polarization delivers secretory granules to the immunological synapse. *Nature* 443: 462–465.
13. Dustin ML, Long EO (2010) Cytotoxic immunological synapses. *Immunol Rev* 235: 24–34.
14. Graf B, Bushnell T, Miller J (2007) LFA-1-mediated T cell costimulation through increased localization of TCR/class II complexes to the central supramolecular activation cluster and exclusion of CD45 from the immunological synapse. *J Immunol* 179:1616–1624.
15. Anikeeva N, et al. (2005) Distinct role of lymphocyte function-associated antigen-1 in mediating effective cytolytic activity by cytotoxic T lymphocytes. *Proc Natl Acad Sci USA* 102:6437–6442.
16. James JR, Vale RD (2012) Biophysical mechanism of T-cell receptor triggering in a reconstituted system. *Nature* 487:64–69.

17. Zhong XS, Matsushita M, Plotkin J, Riviere I, Sadelain M (2010) Chimeric antigen receptors combining 4-1BB and CD28 signaling domains augment PI3kinase/AKT/Bcl-XL activation and CD8+ T cell-mediated tumor eradication. *Mol Ther* 18:413–420.
18. Karlsson H, et al. (2015) Evaluation of intracellular signaling downstream chimeric antigen receptors. *PLoS One* 10:e0144787.
19. Sackstein R, Schatton T, Barthel SR (2017) T-lymphocyte homing: An underappreciated yet critical hurdle for successful cancer immunotherapy. *Lab Invest* 97:669–697.
20. Purbhoo MA, Irvine DJ, Huppa JB, Davis MM (2004) T cell killing does not require the formation of a stable mature immunological synapse. *Nat Immunol* 5:524–530.
21. Huang J, et al. (2013) A single peptide-major histocompatibility complex ligand triggers digital cytokine secretion in CD4(+) T cells. *Immunity* 39:846–857.
22. Zhang M, March ME, Lane WS, Long EO (2014) A signaling network stimulated by β2 integrin promotes the polarization of lytic granules in cytotoxic cells. *Sci Signal* 7: ra96.
23. Mukherjee M, Mace EM, Carisey AF, Ahmed N, Orange JS (2017) Quantitative imaging approaches to study the CAR immunological synapse. *Mol Ther* 25:1757–1768.
24. Lopez JA, et al. (2013) Rapid and unidirectional perforin pore delivery at the cytotoxic immune synapse. *J Immunol* 191:2328–2334.
25. Ma JS, Haydar TF, Radoja S (2008) Protein kinase C delta localizes to secretory lysosomes in CD8+ CTL and directly mediates TCR signals leading to granule exocytosis-mediated cytotoxicity. *J Immunol* 181:4716–4722.
26. Wei Y (2015) On the quest of cellular functions of PEA-15 and the therapeutic opportunities. *Pharmaceuticals (Basel)* 8:455–473.
27. Charo J, et al. (2005) Bcl-2 overexpression enhances tumor-specific T-cell survival. *Cancer Res* 65:2001–2008.
28. Voskoboinik I, Whisstock JC, Trapani JA (2015) Perforin and granzymes: Function, dysfunction and human pathology. *Nat Rev Immunol* 15:388–400.
29. Ritter AT, et al. (2015) Actin depletion initiates events leading to granule secretion at the immunological synapse. *Immunity* 42:864–876.
30. Jenkins MR, Tsun A, Stinchcombe JC, Griffiths GM (2009) The strength of T cell receptor signal controls the polarization of cytotoxic machinery to the immunological synapse. *Immunity* 31:621–631.
31. Chung B, et al. (2014) Antigen-specific inhibition of high-avidity T cell target lysis by low-avidity T cells via trogocytosis. *Cell Rep* 8:871–882.
32. Soares H, et al. (2013) Regulated vesicle fusion generates signaling nanoterritories that control T cell activation at the immunological synapse. *J Exp Med* 210:2415–2433.
33. Gorska MM, Liang Q, Karim Z, Alam R (2009) Uncoordinated 119 protein controls trafficking of Lck via the Rab11 endosome and is critical for immunological synapse formation. *J Immunol* 183:1675–1684.
34. Antón O, et al. (2008) An essential role for the MAL protein in targeting Lck to the plasma membrane of human T lymphocytes. *J Exp Med* 205:3201–3213.
35. Bouchet J, et al. (2017) Rab11-FIP3 regulation of Lck endosomal traffic controls TCR signal transduction. *J Immunol* 198:2967–2978.
36. Kershaw MH, Westwood JA, Darcy PK (2013) Gene-engineered T cells for cancer therapy. *Nat Rev Cancer* 13:525–541.
37. Kawalekar OU, et al. (2016) Distinct signaling of coreceptors regulates specific metabolism pathways and impacts memory development in CAR T cells. *Immunity* 44: 380–390, and erratum (2016) 44:712.
38. Burns WR, Zheng Z, Rosenberg SA, Morgan RA (2009) Lack of specific gammaretroviral vector long terminal repeat promoter silencing in patients receiving genetically engineered lymphocytes and activation upon lymphocyte restimulation. *Blood* 114:2888–2899.
39. Dustin ML, Baldari CT (2017) The immune synapse: Past, present, and future. *Methods Mol Biol* 1584:1–5.
40. Yong CS, et al. (2015) Expression of a chimeric antigen receptor in multiple leukocyte lineages in transgenic mice. *PLoS One* 10:e0140543.
41. Jenkins MR, et al. (2015) Failed CTL/NK cell killing and cytokine hypersecretion are directly linked through prolonged synapse time. *J Exp Med* 212:307–317.
42. Wang LX, et al. (2010) Tumor ablation by gene-modified T cells in the absence of autoimmunity. *Cancer Res* 70:9591–9598.
43. Ritchie ME, et al. (2015) Limma powers differential expression analyses for RNA-sequencing and microarray studies. *Nucleic Acids Res* 43:e47.
44. Smyth GK (2004) Linear models and empirical bayes methods for assessing differential expression in microarray experiments. *Stat Appl Genet Mol Biol* 3:1–25.
45. Lopez JA, et al. (2013) Perforin forms transient pores on the target cell plasma membrane to facilitate rapid access of granzymes during killer cell attack. *Blood* 121: 2659–2668.
46. Tsun A, et al. (2011) Centrosome docking at the immunological synapse is controlled by Lck signaling. *J Cell Biol* 192:663–674.
47. Bertrand F, et al. (2013) An initial and rapid step of lytic granule secretion precedes microtubule organizing center polarization at the cytotoxic T lymphocyte/target cell synapse. *Proc Natl Acad Sci USA* 110:6073–6078.